MATERIALS
CHEMISTRY

FRONTIERS

Check for updates

Incorporation of narcissistic self-sorting supramolecular interactions for the spontaneous fabrication of multiple-color solid-state materials for OLED applications†‡

Yu-Tang Tsai,[a] Guillaume Raffy, [ID][a] Hsiang-Fang Liu,[b] Bo-Ji Peng, [ID][b] Kuo-Pi Tseng,[b] Lionel Hirsch, [ID][c] André Del Guerzo, [ID][a] Dario M. Bassani [ID] *[a] and Ken-Tsung Wong [ID] *[bd]

A series of six compounds composed of an emissive oligofluorene or dithiophenethiobenzimidazole (**p3**) core bearing H-bonding biuret molecular recognition motifs in the *meta*- or *para*-position was investigated with regard to their propensity to undergo either social or narcissistic self-sorting when deposited from dilute THF solutions. The structural similarity of the compounds uniformly leads to social self-sorting with the exception of two combinations involving **p3** for which narcissistic self-sorting is observed instead. Their behavior is attributed to the difference in location of the biuret groups (*meta vs. para*) combined with a greater structural difference in the conjugated core. Deposition of solutions demonstrating narcissistic self sorting gives rise to ensembles of disk-like aggregates exhibiting two different populations of emission (blue and magenta or yellow and orange).

Introduction

Self-sorting is defined as the ability of a multi-component system to undergo spontaneous organization based on a specific property or behavior.[1] It is ubiquitous in living organisms, where it is present at the cellular, sub-cellular, and molecular levels, as well as manifesting itself in the social behaviour of individual organisms.[2] At the molecular scale, self-sorting may be termed narcissistic or social, depending on whether the final outcome results in the grouping of typologically similar (narcissistic self-sorting) or dissimilar molecules (social self-sorting).[3–5] This concept has proven to be particularly useful in understanding and predicting the assembly of molecular sub-components into mixtures of well-defined supramolecular architectures and, in this regard, it bridges the gap between molecular self-assembly and more complex, evolutionary systems based on multi-component libraries.[6,7] Many examples of self-sorting can be found in the assembly of metallo-supramolecular architectures, where ligand structure,[8] metal coordination,[9–11] or stereochemistry[12,13] can impart the resolution of complex mixtures of different metal ions and ligands into a reduced number of more complex structures. Supramolecular assemblies based on complementary ionic forces,[14] H-bonding interactions[15–18] or reversible covalent bond formation[7,19] can also display self-sorting behaviour. Amongst bio-inspired soft-matter materials, orthogonal self-assembly of surfactants may lead to inter-penetrating networks of fibrillar networks[20–25] or to their co-existence with liposomes[26] or liquid crystal bolaamphiphiles, whereas the combination of H-bonding and hydrophobic units can provide self-sorting in micelles.[27]

The concept of self-sorting is crucial for understanding the formation of complex biological systems and carries great potential for bio-organic materials. However, its application to molecular electronics is still rare despite the promise of constructing complex, multi-functional devices from the designed self-assembly of smaller and simpler components.[28–33] Donor–acceptor stacks exhibiting selective charge transfer properties have been obtained by co-crystallization[34] or self-assembly in solution,[35,36] or from organization on surfaces.[37,38] In the case of perylenediimide- and stilbene-based fibrillar networks, self-sorting was shown by small-angle neutron scattering to be sensitive to gelation conditions which also affects inter-component

[a] *Univ. Bordeaux, CNRS, Bordeaux INP, ISM, UMR 5255, F-33400, Talence, France. E-mail: dario.bassani@u-bordeaux.fr*

[b] *Department of Chemistry, National Taiwan University, Taipei, 10617, Taiwan. E-mail: kenwong@ntu.edu.tw*

[c] *IMS, Univ. Bordeaux, Bordeaux INP, ENSCBP, CNRS UMR 5218, F-33400 Talence, France*

[d] *Institute of Atomic and Molecular Science, Academia Sinica, Taipei, 10617, Taiwan*

This journal is © The Royal Society of Chemistry and the Chinese Chemical Society 2020

Mater. Chem. Front., 2020, **4**, 845–850 | 845

electron transfer.[39] Unfortunately, the same forces that induce self-sorting at the molecular level are generally of limited compatibility with the preparation of solution- or vacuum-processed electronic devices. For example, the use of orthogonal molecular recognition motifs may lead to the selective solubilisation or precipitation of one of the components during deposition of the active layer, whereas selection based on the use of long aliphatic chains is not generally conducive towards charge transport. While the interest in exploiting narcissistic molecular self-sorting for photovoltaic applications is obvious, a particularly attractive application of self-sorting would be in the fabrication of OLED devices incorporating pixels of different colours from a single solution of materials.

Our previous work on the use of supramolecular interactions for self-assembled OLED materials led us to the design of electroactive molecules incorporating biuret units.[40] The latter present two orthogonal H-bonding sites and are known to preferentially form sheet-like structures in the solid state. We found the presence of two biuret units at the extremities of a rigid aromatic core to be a general principle guiding the formation of vesicle-like aggregates in organic solvents. Interestingly, the latter are formed spontaneously and can be relatively monodisperse in size (200–500 nm diameter).[41] Upon deposition, evaporation of the solvent leads to the formation of flat disks whose dimensions are determined by the diameter and wall thickness of the aggregate in solution. Thus, disks with diameters of 200–500 nm and only 30–60 nm thick are easily obtained. TEM analysis of the edges of drop-cast samples evidences the formation of multi-walled tubes that undergo constriction to give hollow spheres whose size is directed by the diameter of the tube. Such tubes, formed by rolling up of the H-bonded sheets, would place the H-bonding motifs in the plane of the sphere's surface in agreement with static light scattering results indicating the absence of strong aggregate–aggregate interactions in solution.[41]

Results and discussion

The formation of vesicle-like aggregates from biuret-appended π-conjugated cores is robust, and is a typical case of social self-sorting. Thus, mixing a varying amount of a compound with lower excitation energy gives rise to efficient inter-chromophore energy transfer resulting from fast exciton migration and high density of chromophores. In this fashion, it is possible to obtain aggregates of different colours, including white, by mixing biuret-appended compounds with different emission profiles in solution. The resulting drop- or spin-cast materials possess narrow colour distributions, implying that the dispersion of the components is homogeneous between aggregates. Simultaneously obtaining aggregates of different colours in a single device is therefore not directly possible using this approach and requires either the sequential deposition of the different colours[42,43] or the use of a colour-bleaching technique[44] to subsequently tune the emission profile of the material. Although the size of the rigid, π-conjugated core does

not seem to have a strong effect on the formation of the vesicle-like aggregates, we remarked that this is not the case for the orientation of the biuret molecular recognition motifs. Indeed, reversible conversion between aggregates exhibiting different morphologies (vesicles and fibers) could be obtained through photoisomerization of an azobenezene-containing core. This result prompted us to probe the influence of the connecting point (*meta vs. para*) between the biuret unit and the conjugated chromophore, revealing that some of the components of these two systems can undergo narcisitic self-sorting, which could be used to obtain solid-state OLED devices with pixels of different colors from a single solution of chromophores. We rationalize this behaviour in terms of the packing of molecules within the aggregate shell.

The synthesis of compounds 1–3 in their *para-* and *meta-* series through Suzuki cross-coupling of 3- or 4-biuretphenylboronic acid with the corresponding aromatic core was described previously.[40,44] Both series of compounds spontaneously generate vesicle-like aggregates upon dissolution in anhydrous THF (10^{-4} M concentration) that, upon deposition on conductive substrates, allows the systematic fabrication of OLED devices emitting in the blue, green, and red regions of the visible spectrum.[42,44] Dynamic and static light scattering experiments, and small angle X-ray diffraction are consistent with the presence, in solution, of hollow sphere aggregates possessing a thin (ca. 30 nm) shell that are subject to Brownian motion (*i.e.* that do not interact with one another).[41]

Mixing compounds **p1**–**p3** or **m1**–**m3** in solution results in the deposition of disk-like aggregates that can emit a single colour due to efficient energy migration and transfer processes along with a homogeneous dispersion of the compounds in the aggregates. This is shown in Fig. 1, where the reconstructed colour confocal fluorescence microscope images of the aggregates of pure **m1**, **m2**, and **m3** (calculated from the corrected emission spectra) are shown. From the localization of the emission profiles on the chromatic CIE chart (Fig. 1F), it can be seen that the emissions are very monodisperse and localized in the blue, green, or red areas of the visible region. The emission of **m1**, but containing 1% of **m3** also gives a homogeneous dispersion of aggregates whose emission is localized between the CIE colour coordinates of **m1** and **m3** (Fig. 1D). In the case of **m2** doped with **m3** (10%, Fig. 1E), the emission is now shifted towards the yellow with some small differences between individual aggregates. This is indicative of some narcissistic self-sorting even between such structurally similar compounds (see also Fig. S7 in the ESI‡). The changes in the emission profile in the samples shown in Fig. 1D and E compared to those in Fig. 1A and B are attributed to efficient energy transfer to **m3** from excited **m1** or **m2**, coupled to fast exciton migration in the aggregates. This allows the donor excited state to sample numerous sites, any one of which may undergo radiative energy transfer to a nearby **m3** molecule. Such processes are known to be highly efficient and quenching efficiencies in excess of one acceptor for 100 donors have been observed in fibrillar aggregates.[45]

A similar social self-sorting behaviour is found for most, but not all, combinations of compounds shown in Scheme 1. It is

Fig. 1 Reconstructed colour images of aggregates deposited from solutions (10^{-4} M in THF) of **m1** (A), **m2** (B), and **m3** (C) and of mixtures of **m1** and **m3** (100 : 1, 10^{-4} M in THF, panel (D)) or of mixtures of **m2** and **m3** (100 : 10, 10^{-4} M in THF, panel (E)). The dispersions of colours from the emission of the aggregates from A–C are shown in the CIE chart (F). Images are 20 × 20 μm (λ_{ex} = 375 nm).
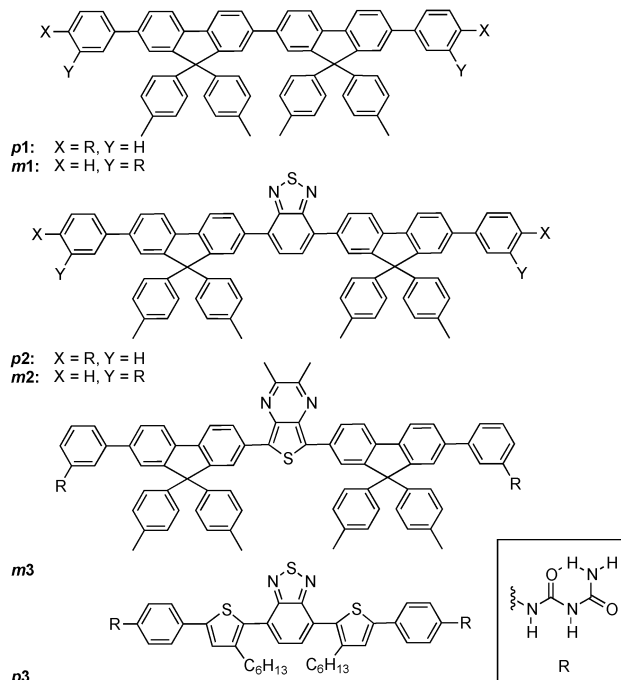
Scheme 1   Structures of compounds used in self-sorting experiments.

Fig. 2 Reconstructed colour image (A) of aggregates deposited from solutions of **m1** and **p3** (100 : 1, 10^{-4} M in THF), and reconstructed colour image (B) of aggregates deposited from solutions of **m2** and **p3** (100 : 10, 10^{-4} M in THF). On the right are shown the CIE plots of the distributions of colours. The inhomogeneous dispersions of **p3** into **m1** or **m2** are examples of narcissistic self-sorting (λ_{ex} = 375 nm).

interesting to note that the combination of **m2** and **m3** gives aggregates that can display a small degree of narcissistic self-sorting despite the similarities of the structures of **m2** and **m3**. The propensity towards narcissistic self-sorting is increased when **m3** is replaced by **p3** (Fig. 2). Thus, blending of **m1** (blue) or **m2** (green) with **p3** (red) gives rise to a mixture of aggregates with a clear two-tone color distribution. In the case of a solution of **m1** and **p3** (100 : 1, 10^{-4} M in THF), a dispersion of blue and magenta aggregates can be observed (Fig. 2A).

Blending of **m2** with **p3** also results in narcissistic self-sorting, as evidenced by the results shown in Fig. 2B. In this case, deposition of a solution containing both **m2** and **p3** (10 : 1, 10^{-4} M in THF) gives rise to a distribution of vesicle-like aggregates that emit in the orange or red region. Although the difference between the two appears small to the naked eye due to its low sensitivity in this region of the spectrum, it is much more apparent in the CIE chromatic diagram showing the distributions of colour pixels. Here, it is clear that the distribution between the two components is much better defined than in the **m1**/**p3** system, giving rise to two distinct emission distribution centred around the emission of each of the two aggregates' emission profiles. However, in contrast to the **m1**/**p3** system, fluorescence lifetime imaging does not reveal significant differences in the emission decay parameters

between the aggregates as these possess a broad distribution of lifetimes centered at *ca.* 5 ns.§

To evaluate the degree of narcissistic self-sorting, we compared the emission spectra of the self-sorted components with those of model systems displaying social self-sorting. In the case of the

---

§ The average lifetimes of **m1**, **m2** and **m3** in the aggregates are 1.6, 3.4 and 2.5 ns, respectively (λ_{ex} = 375 nm).
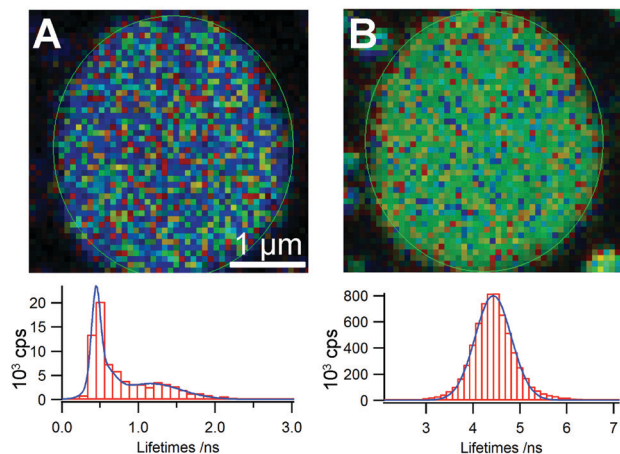
Research Article

Materials Chemistry Frontiers

Fig. 3 Fluorescence lifetime imaging (λ_{ex} = 375 nm) of a single blue-emitting aggregate deposited from solutions of **m1** and **p3** (100 : 1, 10^{-4} M in THF) collected at 400−450 nm (A) or 570−650 nm (B). In (A), only the emission from **m1** is observed and it exhibits a dual distribution of lifetimes in agreement with the existence of regions (blue patches) where no quenching by **p3** is observed. The emission from **p3** (B) shows a single lifetime distribution as expected for direct or sensitized excitation.

m1/p3 system, we selected the **m1/m3** combination as a reference. The absorption and emission profiles of **p3** and **m3** are similar, and we can therefore expect that the efficiency of energy transfer should be comparable. Solutions containing **m1** and **m3** give rise to aggregates for which the emission is homogeneous throughout the sample. Provided that this implies that the concentrations of the components are also homogeneous, this allows us to estimate the relative proportion of each component in the self-sorted vesicles (see the ESI‡ for details). In the case of the **m1/p3** system, we estimate the ratio of the blue to the red component to be 100 : 0.4 and 100 : 9 for the blue and magenta aggregates, respectively. This gives a self-sorting ratio of 9/0.4 = 23. In the case of the **m2/p3** system, a similar analysis gives a composition of green to red component of 100 : 4 and *ca.* 100 : 19 for the orange and red aggregates, respectively.¶ It should be noted, however, that despite the lower self-sorting ratio for the **m2/p3** *vs.* **m1/p3** system, the former has a clearer separation between the colour components resulting from a less broad distribution compared to the **m1/p3** system for which the distribution in colours of the magenta component is significantly broader.

Analysis of the decay kinetics of the donor and acceptor components in the self-sorted vesicles provides additional information concerning how the molecules are organized within individual vesicles. Although single vesicles are close in size to the diffraction-limited resolution of the microscope (*ca.* 200 nm), the distribution of decay constants that is collected reflects the different environments of the emitting species. Thus, in the case of the blue-emitting vesicles in the self-sorted systems of **m1** and **p3** (100 : 1, 10^{-4} M in THF), we find that the decay of **m1** exhibits a dual distribution of

¶ Due to the occurrence of narcissistic self-sorting at higher loadings of **m3**, the proportion of **m2** to **p3** in the red vesicles was estimated from extrapolation of the data from **m2** and **m3** at lower loading ratios.

lifetimes indicating that the environment of **m1** inside the vesicle is not uniform (Fig. 3). One of the distributions, centered at *ca.* 1.3 ns, is similar to that of the unquenched species, which we attribute to the presence of patches of pure or nearly-pure **m1** in the vesicle. The shorter component is instead attributed to regions of the vesicles in which some **p3** is present, resulting in quenching of the emission. Not unexpectedly, imaging the lifetime distribution on the vesicle surface area does not readily reveal regions in which different domains are visible as these would be below the instrumental resolution. Analysis of the acceptor decay kinetics shows the expected symmetrical distribution of lifetimes centred at the mean lifetime of the unquenched acceptor (4–5 ns). In the case of the **m2/p3** system, unsymmetrical decay distributions are also seen, but the overlap in emission between the donor and acceptor does not allow us to acquire and analyse each decay component individually.

The origin of the self-sorting behaviour of only a few of the 12 possible combinations is intriguing. Clearly, the location of the biuret motif (*meta vs. para*) is important, since varying only the core (*e.g.* **p1/p3** or **p2/p3**) does not lead to significant self-sorting despite the identical difluorene-based chromophores used for **1** and **2**. Likewise, only varying the point of attachment is not sufficient since not all of the *para/meta* combinations give rise to self-sorting. Our previous investigations of the self-assembly process in solution are consistent with a model in which the shell of the vesicles is composed of molecules that are oriented with their long axis parallel to the surface.[41] This would favour H-bonding resulting from ordered packing of the molecules. It is plausible that self-sorting results from the difference in packing arrangement of the **p3** molecules with respect to the **m1** and **m2** compounds due to the combined difference in the position of the biuret and the structure of the core.

Conclusions

The spontaneous aggregation behavior of a series of rigid chromophores appended with biuret H-bonding motifs provides examples of both social and narcissistic self-sorting. The former is more pronounced, as would be expected based on the structural similarity of the molecular constituents. This results in the formation of disk-like aggregates whose emission envelope was previously shown to be tunable over the visible range of the spectrum. Interestingly, even a minor structural modification resulting from exchanging a benzothiodiazole with a thienopyriazene spacer (**m2** *vs.* **m3**) inside the hexaphenyl aromatic core is sufficient to induce a small degree of narcissisitic self-sorting. This is amplified by changing the point of attachment of the biuret molecular recognition motif, which results in some systems displaying stronger narcissistic self-sorting behaviour. Such sensitivity to the molecular structure is likely the result of structural order in the vesicle shell that is itself highly dependent on molecular structure. Prediction of which structural modification will lead to a specific sorting behaviour remains, however, elusive at present. Even so, this behaviour can give

848 | *Mater. Chem. Front.*, 2020, **4**, 845–850

This journal is © The Royal Society of Chemistry and the Chinese Chemical Society 2020

rise to the spontaneous formation of side-by-side aggregates emitting different colors from deposition of a single solution of both components. This approach could provide a solution to mitigate the effect of colour bleeding in the fabrication of OLEDs, which is a limiting factor in determining the resolution and brightness of commercial devices. In this respect, this example represents an important achievement by demonstrating the importance of even minor changes in the molecular structure.

Conflicts of interest

There are no conflicts to declare.

Acknowledgements

Notes and references

1 J.-M. Lehn, *Science*, 2002, **295**, 2400–2403.
2 A. Wu and L. Isaacs, *J. Am. Chem. Soc.*, 2003, **125**, 4831–4835.
3 R. Kramer, J. M. Lehn and A. Marquis-Rigault, *Proc. Natl. Acad. Sci. U. S. A.*, 1993, **90**, 5394.
4 M. J. Mayoral, C. Rest, J. Schellheimer, V. Stepanenko and G. Fernandez, *Chemistry*, 2012, **18**, 15607–15611.
5 P. N. Taylor and H. L. Anderson, *J. Am. Chem. Soc.*, 1999, **121**, 11538–11545.
6 J.-F. Ayme and J.-M. Lehn, *Adv. Inorg. Chem.*, 2018, **71**, 3–78.
7 M. Kolodziejski, A. R. Stefankiewicz and J.-M. Lehn, *Chem. Sci.*, 2019, **10**, 1836–1843.
8 J. M. Lehn, A. Rigault, J. Siegel, J. Harrowfield, B. Chevrier and D. Moras, *Proc. Natl. Acad. Sci. U. S. A.*, 1987, **84**, 2565–2569.
9 J. Zhong, L. Zhang, D. P. August, G. F. S. Whitehead and D. A. Leigh, *J. Am. Chem. Soc.*, 2019, **141**, 14249–14256.
10 W. M. Bloch and G. H. Clever, *Chem. Commun.*, 2017, **53**, 8506–8516.
11 F. De Campo, D. Lastecoueres, J.-M. Vincent and J.-B. Verlhac, *J. Org. Chem.*, 1999, **64**, 4969–4971.
12 D. M. Bassani, J.-M. Lehn, K. Fromm and D. Fenske, *Angew. Chem., Int. Ed.*, 1998, **37**, 2364–2367.
13 I. Pianet and J.-M. Vincent, *Inorg. Chem.*, 2004, **43**, 2947–2953.
14 S.-J. Rao, Q. Zhang, J. Mei, X.-H. Ye, C. Gao, Q.-C. Wang, D.-H. Qu and H. Tian, *Chem. Sci.*, 2017, **8**, 6777–6783.
15 D. Ajami, J.-L. Hou, T. J. Dale, E. Barrett and J. Rebek, Jr., *Proc. Natl. Acad. Sci. U. S. A.*, 2009, **106**, 10430–10434.
16 D. S. Philips, K. K. Kartha, A. T. Politi, T. Krueger, R. Q. Albuquerque and G. Fernandez, *Angew. Chem., Int. Ed.*, 2019, **58**, 4732–4736.

17 A. Nuthanakanti, M. B. Walunj, A. Torris, M. V. Badiger and S. G. Srivatsan, *Nanoscale*, 2019, **11**, 11956–11966.
18 S. Schoder and C. A. Schalley, *Chem. Commun.*, 2017, **53**, 9546–9549.
19 K. Acharyya and P. S. Mukherjee, *Angew. Chem., Int. Ed.*, 2019, **58**, 8640–8653.
20 Y. Wang, M. Lovrak, Q. Liu, C. Maity, V. A. A. le Sage, X. Guo, R. Eelkema and J. H. van Esch, *J. Am. Chem. Soc.*, 2019, **141**, 2847–2851.
21 Y. Wang, R. M. de Kruijff, M. Lovrak, X. Guo, R. Eelkema and J. H. van Esch, *Angew. Chem., Int. Ed.*, 2019, **58**, 3800–3803.
22 W. Tanaka, H. Shigemitsu, T. Fujisaku, R. Kubota, S. Minami, K. Urayama and I. Hamachi, *J. Am. Chem. Soc.*, 2019, **141**, 4997–5004.
23 B. O. Okesola, Y. Wu, B. Derkus, S. Gani, D. Wu, D. Knani, D. K. Smith, D. J. Adams and A. Mata, *Chem. Mater.*, 2019, **31**, 7883–7897.
24 G. Liu, C. Zhou, W. L. Teo, C. Qian and Y. Zhao, *Angew. Chem., Int. Ed.*, 2019, **58**, 9366–9372.
25 E. R. Draper and D. J. Adams, *Nat. Chem.*, 2016, **8**, 737–738.
26 J. Boekhoven, A. M. Brizard, M. C. A. Stuart, L. Florusse, G. Raffy, A. Del Guerzo and J. H. van Esch, *Chem. Sci.*, 2016, **7**, 6021–6031.
27 A. Pal, S. Karthikeyan and R. P. Sijbesma, *J. Am. Chem. Soc.*, 2010, **132**, 7842–7843.
28 H. Kar and S. Ghosh, *Isr. J. Chem.*, 2019, **59**, 881–891.
29 K.-T. Wong and D. M. Bassani, *NPG Asia Mater.*, 2014, **6**, e116.
30 E. R. Draper, B. Dietrich and D. J. Adams, *Chem. Commun.*, 2017, **53**, 1864–1867.
31 E. R. Draper, J. R. Lee, M. Wallace, F. Jackel, A. J. Cowan and D. J. Adams, *Chem. Sci.*, 2016, **7**, 6499–6505.
32 X. Feng, L. Chen, Y. Honsho, O. Saengsawang, L. Liu, L. Wang, A. Saeki, S. Irle, S. Seki, Y. Dong and D. Jiang, *Adv. Mater.*, 2012, **24**, 3026–3031.
33 W.-C. Geng, Y.-C. Liu, Y.-Y. Wang, Z. Xu, Z. Zheng, C.-B. Yang and D.-S. Guo, *Chem. Commun.*, 2016, **53**, 392–395.
34 M. A. Niyas, R. Ramakrishnan, V. Vijay and M. Hariharan, *Chem. – Eur. J.*, 2018, **24**, 12318–12329.
35 V. S. Nair, R. D. Mukhopadhyay, A. Ajayaghosh, A. Saeki and S. Seki, *Sci. Adv.*, 2016, **2**, e1600142.
36 C.-H. Huang, N. D. McClenaghan, A. Kuhn, J. W. Hofstraat and D. M. Bassani, *Org. Lett.*, 2005, **7**, 3409–3412.
37 N.-T. Lin, A. Vargas Jentzsch, L. Guenee, J.-M. Neudoerfl, S. Aziz, A. Berkessel, E. Orentas, N. Sakai and S. Matile, *Chem. Sci.*, 2012, **3**, 1121–1127.
38 A. Mendez-Ardoy, N. Markandeya, X. Li, Y.-T. Tsai, G. Pecastaings, T. Buffeteau, V. Maurizot, L. Muccioli, F. Castet, I. Huc and D. M. Bassani, *Chem. Sci.*, 2017, **8**, 7251–7257.
39 E. R. Cross, S. Sproules, R. Schweins, E. R. Draper and D. J. Adams, *J. Am. Chem. Soc.*, 2018, **140**, 8667–8670.
40 K.-P. Tseng, F.-C. Fang, J.-J. Shyue, K.-T. Wong, G. Raffy, G. A. Del and D. M. Bassani, *Angew. Chem., Int. Ed.*, 2011, **50**, 7032–7036.

This journal is © The Royal Society of Chemistry and the Chinese Chemical Society 2020

Mater. Chem. Front., 2020, **4**, 845–850 | **849**

41 S. K. P. Velu, M. Yan, K.-P. Tseng, K.-T. Wong, D. M. Bassani and P. Terech, *Macromolecules*, 2013, **46**, 1591–1598.

42 Y.-T. Tsai, K.-P. Tseng, Y.-F. Chen, C.-C. Wu, G.-L. Fan, K.-T. Wong, G. Wantz, L. Hirsch, G. Raffy, A. Del Guerzo and D. M. Bassani, *ACS Nano*, 2016, **10**, 998–1006.

43 K.-P. Tseng, Y.-T. Tsai, J.-J. Shyue, G. Raffy, A. Del Guerzo, K.-T. Wong and D. M. Bassani, *Chem. Phys. Lett.*, 2017, **683**, 43–48.

44 Y.-T. Tsai, H.-F. Liu, B.-J. Peng, K.-P. Tseng, M.-C. Kuo, K.-T. Wong, G. Wantz, L. Hirsch, G. Raffy, A. Del Guerzo and D. M. Bassani, *ACS Appl. Mater. Interfaces*, 2017, **9**, 36045–36052.

45 C. Giansante, G. Raffy, C. Schäfer, H. Rahma, M.-T. Kao, A. G. L. Olive and A. D. Guerzo, *J. Am. Chem. Soc.*, 2011, **133**, 316–325.

This journal is © The Royal Society of Chemistry and the Chinese Chemical Society 2020